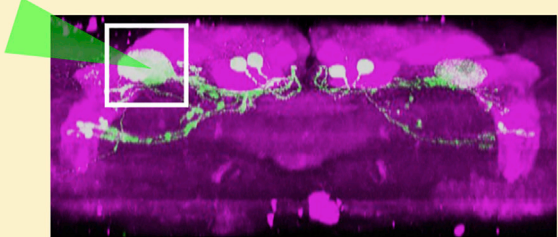


Article

# Imaging through the Whole Brain of *Drosophila* at $\lambda/20$ Super-resolution

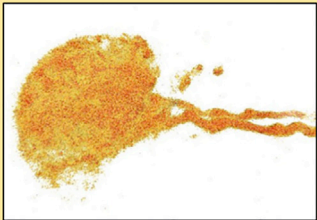
**Target**

Dense Structure In Thick Tissue

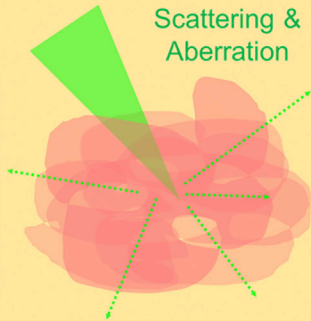


**Issues**

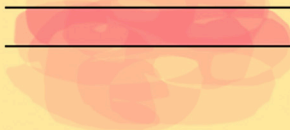
Insufficient resolution



Scattering & Aberration

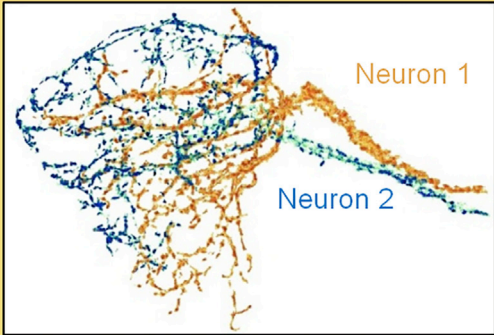


Need Optical Sectioning



**Solutions**

Superresolution  
+  
Tissue Clearing  
+  
Spinning disk confocal



Han-Yuan Lin, Li-An Chu, Hsuan Yang, ..., Keng-Hui Lin, Shi-Wei Chu, Ann-Shyn Chiang

kenghui@gate.sinica.edu.tw (K.-H.L.)  
swchu@phys.ntu.edu.tw (S.-W.C.)  
aschiang@life.nthu.edu.tw (A.-S.C.)

**HIGHLIGHTS**

Spatial resolution of 20 nm at  $\sim 200 \mu\text{m}$  imaging depth (may be extended)

Super-resolution tracking of densely entangled neural fibers in an intact brain

All tools (FP, confocal, clearing, localization) are commercially available

Lin et al., iScience 14, 164–170  
April 26, 2019 © 2019 The Authors.  
<https://doi.org/10.1016/j.isci.2019.03.025>



## Article

Imaging through the Whole Brain of *Drosophila* at  $\lambda/20$  Super-resolution

Han-Yuan Lin,<sup>1,8</sup> Li-An Chu,<sup>2,3,8</sup> Hsuan Yang,<sup>3</sup> Kuo-Jen Hsu,<sup>1,2</sup> Yen-Yin Lin,<sup>2</sup> Keng-Hui Lin,<sup>3,\*</sup> Shi-Wei Chu,<sup>1,4,9,\*</sup> and Ann-Shyn Chiang<sup>2,3,5,6,7,\*</sup>

## SUMMARY

Recently, many super-resolution technologies have been demonstrated, significantly affecting biological studies by observation of cellular structures down to nanometer precision. However, current super-resolution techniques mostly rely on wavefront engineering or wide-field imaging of signal blinking or fluctuation, and thus imaging depths are limited due to tissue scattering or aberration. Here we present a technique that is capable of imaging through an intact *Drosophila* brain with 20-nm lateral resolution at  $\sim 200 \mu\text{m}$  depth. The spatial resolution is provided by molecular localization of a photoconvertible fluorescent protein Kaede, whose red form is found to exhibit blinking state. The deep-tissue observation is enabled by optical sectioning of spinning disk microscopy, as well as reduced scattering from optical clearing. Together these techniques are readily available for many biologists, providing three-dimensional resolution of densely entangled dendritic fibers in a complete *Drosophila* brain. The method paves the way toward whole-brain neural network studies and is applicable to other high-resolution bioimaging.

## INTRODUCTION

Fluorescence microscopy is an indispensable tool in biomedical studies because it provides molecular information to be located within cells or tissues spatially and temporally. In the last decade, significant improvement of optical resolution beyond diffraction limit based on fluorescence microscopy has been realized (Huang et al., 2010), down to nanometer or even angstrom scales recently (Weisenburger et al., 2017). These techniques rely on either wavefront engineering or wide-field imaging of signal blinking or fluctuation (Huang et al., 2010), and thus are not able to enhance resolution inside thick tissue due to scattering, aberration, and out-of-focus signals. One particularly strong motivation for thick-tissue super-resolution is the urgent need to map the neuronal network and connectivity at dendritic level throughout a whole intact brain with high enough spatial resolution to understand brain functions.

There have been lots of recent efforts to enhance spatial resolution in deep tissue. For example, localization microscopy combined with temporal focusing (TF) (Vaziri et al., 2008) or (two-photon) light sheet (Chen et al., 2016; Zanicchi et al., 2011) provides optical sectioning for excitation, but the scattering-induced cross talk in space due to the wide-field detection scheme limits the thickness of the samples to be less than 100  $\mu\text{m}$ . Another wide-field-based technique, structured illumination microscopy (SIM), exhibits similar issues on both excitation and detection. Even when combined with a line scan confocal scheme, the imaging depth of SIM is still limited to 20  $\mu\text{m}$  (Schropp et al., 2017). On the other hand, stimulated emission depletion (STED), reversible saturable optical linear fluorescence transitions (RESOLFT), and saturated excitation (SAX) microscopies, which are based on a point scan confocal geometry and reduce the spatial cross talk, are demonstrated to achieve super-resolution at tens of micrometers imaging depth (Schnorrenberg et al., 2016; Takasaki et al., 2013; Yamanaka et al., 2013). The key is to maintain a consistent beam shape deep inside the sample. For example, the imaging depth of STED is enhanced to about 100  $\mu\text{m}$  in a cell aggregate by using a correction collar to minimize spherical aberration (Urban et al., 2011). Recently, a hollow Bessel beam STED reported 100-nm resolution at imaging depth of 155  $\mu\text{m}$  in an agarose sample, which is highly transparent (Yu et al., 2016). Although STED and RESOLFT seem to be more promising for tissue imaging, their resolutions are in general on the order of 60–100 nm, i.e., less resolving power than the localization approaches. One recent innovation is to expand the tissue, to achieve simultaneous clearing and resolution enhancement (Chang et al., 2017; Chen et al., 2015a; Ku et al., 2016). Nevertheless, the effective imaging depth is thus reduced, and the expansion techniques do not provide increasing ratio of depth and resolution. Thus, a better strategy is to combine localization with optical sectioned detection, such as line scan confocal microscopy (Lee et al., 2012). However, the reported

<sup>1</sup>Department of Physics, National Taiwan University, Taipei 10617, Taiwan

<sup>2</sup>Brain Research Center, National Tsing Hua University, Hsinchu 30013, Taiwan

<sup>3</sup>Institute of Physics, Academia Sinica, Taipei 11529, Taiwan

<sup>4</sup>Molecular Imaging Center, National Taiwan University, Taipei 10617, Taiwan

<sup>5</sup>Institute of Systems Neuroscience, National Tsing Hua University, Hsinchu 30013, Taiwan

<sup>6</sup>Institute of Molecular and Genomic Medicine, National Health Research Institutes, Zhunan, Miaoli 35053, Taiwan

<sup>7</sup>Kavli Institute for Brain and Mind, University of California, San Diego, La Jolla, CA 92093-0526, USA

<sup>8</sup>These authors contributed equally

<sup>9</sup>Lead Contact

\*Correspondence: kenghui@gate.sinica.edu.tw (K.-H.L.), swchu@phys.ntu.edu.tw (S.-W.C.), aschiang@life.nthu.edu.tw (A.-S.C.)

<https://doi.org/10.1016/j.isci.2019.03.025>



resolution-depth performance of this combination is 60-nm spatial resolution at 80  $\mu\text{m}$  depth, which is comparable to other methods.

In this work, we utilized spinning disk confocal microscopy, which is commercially available and widely used in biology, to reject out-of-focus fluorescence (Uno et al., 2014). The spatial resolution and penetration depth are simultaneously enhanced by combination of molecular localization and optical clearing (Liu and Chiang, 2003). With the aid of a blinking fluorescent protein, Kaede (Ando et al., 2002), which can be expressed in neurons of interests, we demonstrated that confocal localization deep imaging with optical clearing (COOL) can reach less than  $\lambda/20$  lateral resolution at nearly 200  $\mu\text{m}$  depth inside an intact *Drosophila* brain, which is the highest record of depth-over-resolution ratio reported to date in the literature. The combination of resolution and imaging depth provides a potential route to map the neural network among the densely packed 100,000 neurons in the whole brain at high resolution.

## RESULTS

### Optical Sectioned Observation of Blinking Fluorescent Protein Kaede

Figures 1A and 1B show the comparison between conventional wide-field and spinning-disk confocal imaging on the same G0239-Gal4 neurons, which express Kaede fluorescent protein, in a *Drosophila* brain (see Supplemental Information for sample preparation) (Pai et al., 2013). As expected, the wide-field modality loses contrast within less than 50  $\mu\text{m}$  depth, even if the brain was mounted in a clearing reagent, whereas confocal works well all the way into the brain. The images acquired by the spinning-disk confocal microscope demonstrate high quality of blinking fluorescence spots for localization, whose example is given in Figure 1C (see Video S1 for blinking fluorescence spots in deep tissue).

As a photoconvertible fluorescent protein, it is no surprise that Kaede has been used in photoactivatable localization microscopy (PALM) (Betzig et al., 2006). However, please note that the blinking in Video S1 is not based on photoconversion. Here we found that the red form, or photoconverted form, of this photoconvertible fluorescent protein exhibits a blinking state, which has not been reported before. Its blinking properties are presented in Transparent Methods. The brightness of the blinking state is enough to enable  $\sim 20$ -nm spatial resolution. Similar to all localization-based techniques, by accumulating images over time, a comprehensive map of fluorophore distribution is unraveled.

### Resolution Enhancement in the Top and Bottom of an Intact Brain

This set of experiment is done in two different Gal4 lines, namely, G0239-Gal4 cells and krasavietz-Gal4 cells (see Figure S3 for these neuron morphologies and the areas for imaging). The former neuron is just below the surface of the brain, whereas the latter is located at the bottom of the brain. Therefore the selection of these two neurons provides a control group to examine resolution enhancement at different depths of an intact *Drosophila* brain.

Figures 1D and 1E demonstrate the significantly enhanced spatial resolution by COOL microscopy at the surface of brain. The cross-sectional profile of one dendrite is given in Figure 1F. Quantitatively, with the spinning disk confocal system, the full-width-at-half-maximum is about  $408 \pm 35$  nm, whereas that of COOL is  $80.8 \pm 4.2$  nm (statistics in Figure S1 and Table S1), which presents the real diameter of a dendrite inside the *Drosophila* brain (Pai et al., 2013). The spatial resolution of COOL is determined by the uncertainty of localization, i.e.,  $25.2 \pm 9.8$  nm (see Figure S2), which is 15 times better than the confocal resolution.

Please note that conventional wide-field localization techniques also provide resolution enhancement at the sample surface, thus the main impact of COOL microscopy is to achieve super-resolution inside a thick tissue. This capability is demonstrated in Figures 1G and 1H, which are acquired at the bottom of a *Drosophila* brain, namely, the dendrite network of krasavietz-Gal4 cells (Dubnau et al., 2003). As expected, the confocal microscopy shows a blurred image of the densely distributed neuropil, whereas the COOL modality provides high-contrast and high-resolution visualization of the dendrite network. The quantitative value in Figure 1I and the corresponding statistical analysis in Figure S2 indicate that the localization uncertainty is  $21.6 \pm 10.1$  nm at this depth, manifesting that resolution enhancement down to less than  $\lambda/20$  is consistently obtained throughout the whole brain. Figures 1J and 1K show that two adjacent dendrites can only be resolved by COOL microscopy. The  $\sim 20$ -nm spatial resolution is necessary to distinguish tightly entangled neurites, whose minimal separation is two times the thickness of a cell membrane, i.e., 10 nm, when a fluorescent protein is expressed in cytosol.

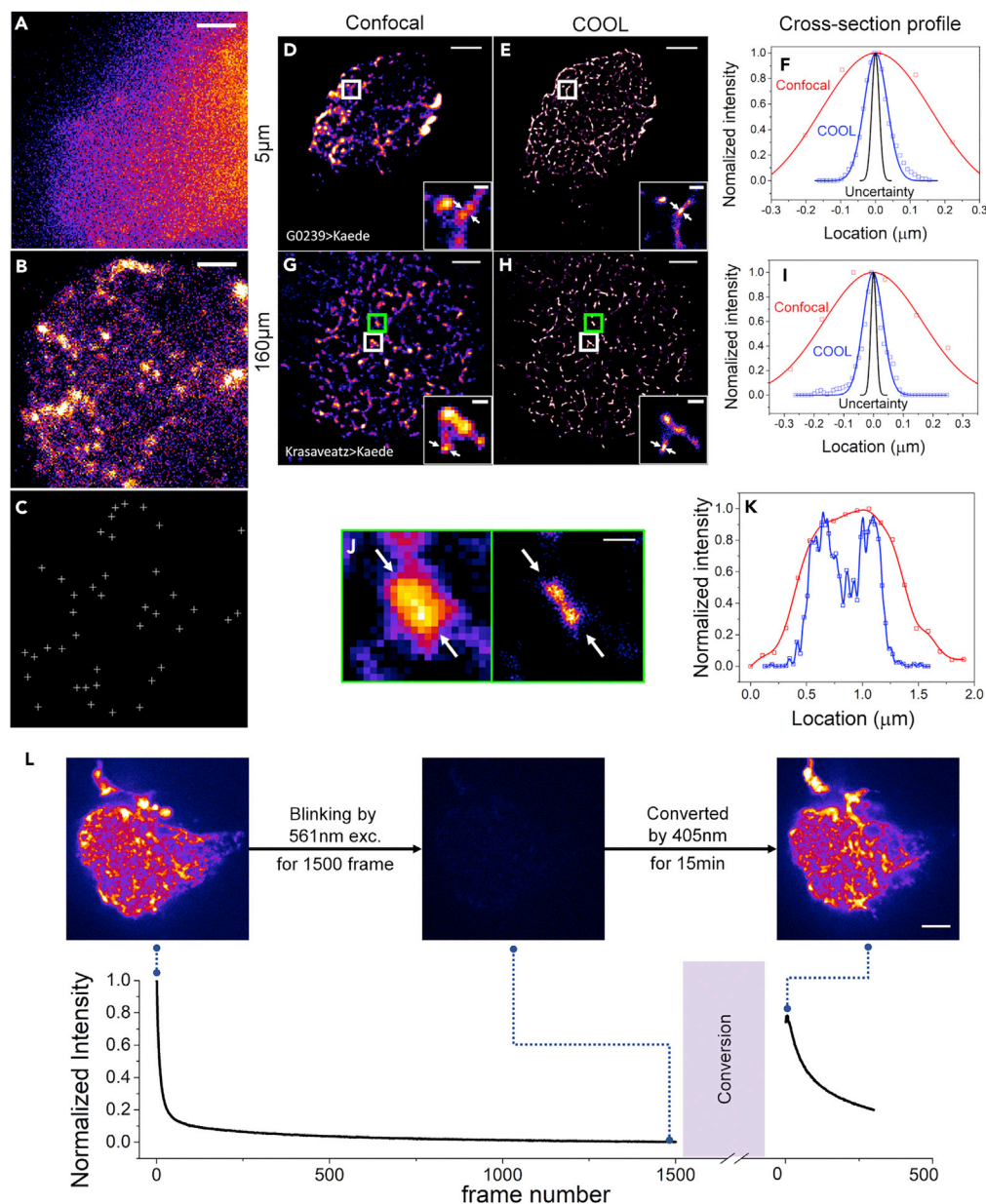


**Figure 1. Optical Sectioned Detection and Resolution Enhancement of COOL**

(A) Wide-field image of a *Drosophila* brain at 45  $\mu\text{m}$  depth. No detail is visible due to out-of-focus fluorescence.

(B) Spinning-disk confocal image of the same sample at 70  $\mu\text{m}$  depth. The axial contrast is greatly improved.

(C) Localized fluorescence spots of (B).

(D–I) (D–F) Resolution enhancement of COOL at 5  $\mu\text{m}$  depth and (G–I) at 160  $\mu\text{m}$  depth. The insets are zoom-in views of white squares, and arrows mark the region corresponding to the profiles. In (F), the values of full-width-at-half-maximum of confocal, COOL, and localization uncertainty are 374, 77.8, and 25.2 nm, respectively. In (I), at the bottom of the brain, the corresponding numbers are 388, 78.4, and 21.6 nm, respectively, demonstrating that the super-resolution is maintained throughout the whole brain.

(J and K) (J) Zoom-in of the green squares in (G and H) and the corresponding profiles in (K) show clear separation of two dendrites by COOL.

(L) An extraordinary advantage of Kaede is its photoconvertibility. During the blinking image acquisition, the red form of Kaede gradually bleaches, as shown by the middle image and the temporal evolution curve in the bottom. The right-hand-side image shows that photoconversion of the abundant green form of Kaede by a 405-nm laser effectively replenishes the blinking red form for subsequent super-resolution imaging.

Cells for demonstration: (A–E, L) G0239-Gal4 cells and (G–J) krasavietz-Gal4 cells. Scale bars: 3  $\mu\text{m}$  in (A–C); 5  $\mu\text{m}$  in images and 500 nm in insets in (D, E, G, and H); 500 nm in (J); 500 nm, (L); and 5  $\mu\text{m}$  in (I).

### Photoconversion to Replenish Blinking Fluorophores

An additional highlight of the technique lies in the photoconvertibility of Kaede, which allows replenishment of the blinking red form with the aid of a 405-nm laser, as demonstrated in Figure 1L (see Figure S4 for a control experiment showing that the red form of Kaede does not increase without 405-nm illumination). One major issue in most super-resolution microscopy is the bleaching of fluorophores under high-intensity illumination, resulting in structure discontinuity, and photoconvertibility potentially helps to solve this issue.

### Volumetric Tracing of Densely Entangled Dendritic Fibers

The optical sectioned 20-nm resolution throughout a whole brain provides unprecedented opportunity to distinguish closely intertwined neurons in three dimensions. One nice example is the G0239-Gal4 neurons (Pai et al., 2013), which consists of two neurons in each side of the brain, and their dendritic fibers densely entangle into a complex network extending tens of micrometers. Here we show that COOL is able to unravel the neurite distribution, as shown in Figure 2. Figure 2A presents sequential images in the axial direction with COOL and confocal modalities. The arrowheads illustrate how to identify a dendrite twist in three-dimensions with COOL. The correspondingly reconstructed dendrite network is given in Figure 2B, with color marked on individual dendrites. It is apparent that only with the exceptional combination of spatial resolution, penetration depth, and optical sectioning of COOL the two three-dimensional (3D) intertwined dendrites can be discriminated without additional genetic manipulation, but this is not possible with either confocal or conventional localization microscopy. Figure 2C shows a large-scale separation of dendritic branches between the two cells of G0239-Gal4 (see Video S3 for the 3D view and Figure S5 for discussion with confocal and electron microscopy). These results demonstrate the potential of COOL toward constructing whole-brain neural networks even with the unusually thin dendrites in *Drosophila*.

## DISCUSSION

We have demonstrated localization microscopy at unprecedented depth in this study, with the aid of high-speed confocal setup, a blinking fluorescent protein, and optical clearing. The depth-resolution comparison of various state-of-the-art techniques are summarized in Figure 3. The COOL techniques are marked with a red star, which is located at the upper-left corner of the plot, i.e., the most wanted corner. To compare with other deep-tissue super-resolution techniques, the figure of merit can be defined as the ratio of imaging depth over spatial resolution. As shown in the right panel of Figure 3, COOL apparently provides the state-of-the-art performance over all other methods. Please note that the current 160- $\mu\text{m}$  imaging depth represents the thickness of the *Drosophila* brain, not depth limit. As the super-resolution does not degrade throughout the whole brain, the COOL technique could be potentially applied to much thicker samples.

One particular advantage of COOL comes from commercially available tools such as spinning disk confocal microscope and genetically controllable blinking proteins, thus facilitating easy access among biologists. The ability to resolve neuronal fine structures in intact animal brain below diffraction limit opens the possibility to unravel biological questions such as neuron morphological structure on a nanometer scale, as well as protein distribution on the synapses due to memory formation or loss, aging, social interactions, etc.

In summary, we have achieved an unprecedented combination of 20-nm lateral resolution in  $\sim 200\text{-}\mu\text{m}$ -deep tissue samples, based on amalgamation of key technologies, including spinning disk confocal, localization microscopy, optical clearing, and a blinking fluorescent protein. The photoconvertible fluorescent protein enables sequential conversion into blinking forms, to facilitate neural tracing in a dense network. The technologies are readily available for many biologists without the need of upgrading hardware. This method can be widely used not only for brain neural network studies but also for other high-resolution imaging in biological tissues and cells.

### Limitations of the Study

There are several limitations in the current design. First, the axial resolution is still diffraction-limited to about 1  $\mu\text{m}$  due to the spinning disk confocal design. The axial resolutions of various super-resolution techniques have been well documented, and in our case (Sahl et al., 2017), they can be further enhanced by incorporating point-spread function engineering (Diezmann et al., 2016) into the spinning disk system. Second, the Kaede fluorescent protein requires a toxic chemical  $\beta$ -mercaptoethanol (BME) to stimulate its blinking (see sample preparation in the Transparent Methods), and FocusClear does not work for live tissue, so currently it is not possible for in vivo observation. However, we would like to point out that the

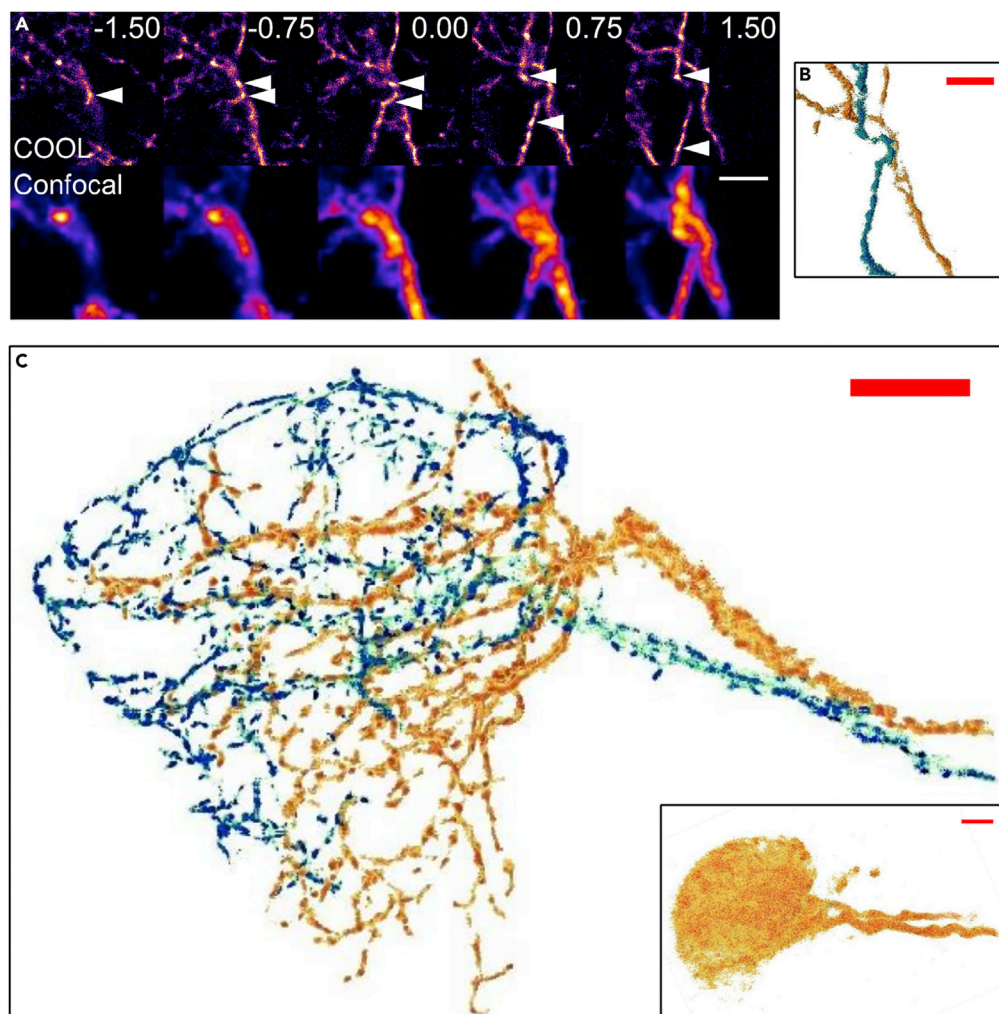


### Figure 2. Three-Dimensional Imaging and Reconstruction to Trace Deep-Brain Neurites with Unprecedented Resolution

(A and B) (A) COOL (top) and confocal (bottom) images across two intertwined dendrites of V3 neurons. Numbers indicate the relative depth ( $\mu\text{m}$ ) of image. The arrowheads indicate the endpoints of a specific neurite at different optical sections, enabling the subsequent 3D reconstruction of the green-colored dendrite in (B). Different colors indicate individual dendrites (see [Video S2](#) for 3D view).

(C) 3D reconstruction of super-resolved complete dendritic network of G0239-Gal4 (see raw data in [Video S3](#), segmentation in [Video S4](#), and 3D view in [Video S5](#)). Two colors indicate that the fibers are from two different cells. The inset shows 3D confocal image from the same neuron, manifesting that the dense dendritic arbor cannot be resolved. Scale bars:  $3 \mu\text{m}$  in (A and B) and  $5 \mu\text{m}$  in (C and its inset). The axial step is  $0.75 \mu\text{m}$ , and the image thickness is  $6 \mu\text{m}$  in (B) and  $28 \mu\text{m}$  in (C).

spinning disk system is suitable for live brain studies, with reasonable penetration capability. Therefore finding a proper agent for live-tissue clearing ([Zhu et al., 2013](#)) as well as photoactivatable proteins that blink in live-cell conditions will enable 3D super-resolution in a live brain.

Third, the imaging speed is limited by the brightness and blinking rate of the fluorophores, and can be further improved by optimizing laser power and the density of activated fluorescent protein at each frame ([Fox-Roberts et al., 2017](#)). It is possible to achieve one super-resolved frame within a split second ([Dertinger et al., 2009](#); [Jones et al., 2011](#)). Last but not least, the neurite fiber distribution is identified manually now. It will be a necessary next step to develop an auto-tracking program to find out dendritic tree divisions and locations of neurite terminals and synapses.

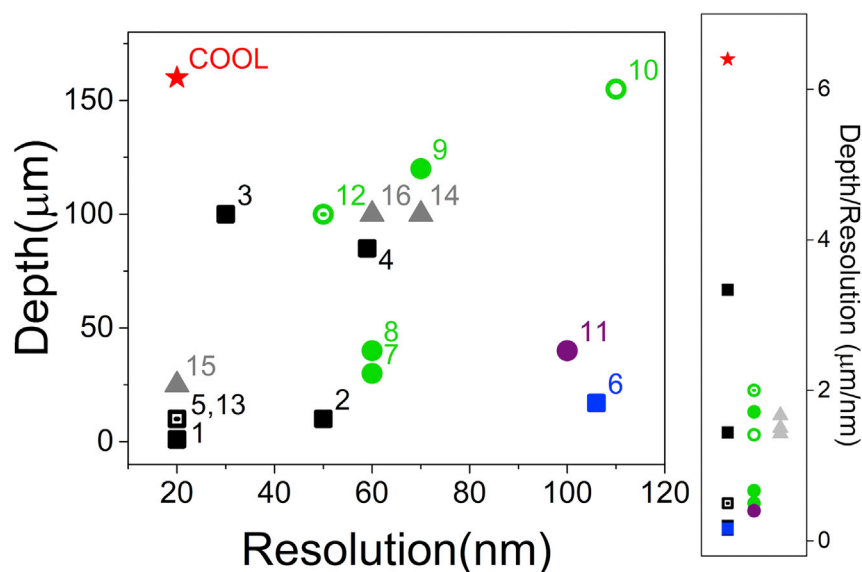


**Figure 3. Comparison of Reported Deep-Tissue Super-Resolution Techniques with 100-nm or Better Resolution**

Wide-Field techniques are marked in squares (localization microscopy: 1–5 and 13 as black squares; SIM: 6 as blue square), scanning-based techniques are in circles (STED/RESOLFT: 7–10 and 12 as green circles; SAX: 11 as purple circle), sample expansion techniques are in gray triangles (14–16), and COOL is the star. In general, localization-based methods (black squares) provide better resolution, whereas scanning-based methods (circles) offer better imaging depth. Right panel: comparison of figures of merit (image depth over resolution) among various techniques. (1) Traditional localization microscope (Rust et al., 2006). (2) Combination of TF and localization microscope (Vaziri et al., 2008). (3) Combination of light sheet and PALM (Zanacchi et al., 2011). (4) Combination of line scan confocal and localization microscope (Lee et al., 2012). (5) Spinning disk confocal localization without clearing (the points 5 and 13 overlap together) (Schueder et al., 2017). (6) Hexagonal line-confocal SIM (Schropp et al., 2017). (7) Two-photon excitation with pulsed STED depletion (Takasaki et al., 2013). (8) RESOLFT (Schnorrenberg et al., 2016). (9) STED with aberration-reducing optics (Urban et al., 2011). (10) Hollow Bessel beam depletion STED in agarose (Yu et al., 2016). (11) SAX (Yamanaka et al., 2013). (12) Combination of tissue clearing and STED (Ke et al., 2016). (13) Combination of tissue clearing and localization microscopy (Ke et al., 2016). (14) Expansion microscopy (Chen et al., 2015a). (15) Iterative expansion microscopy (Chang et al., 2017). (16) Magnified analysis of the proteome (Ku et al., 2016).

## METHODS

All methods can be found in the accompanying [Transparent Methods supplemental file](#).

## SUPPLEMENTAL INFORMATION

Supplemental Information can be found online at <https://doi.org/10.1016/j.isci.2019.03.025>.

## ACKNOWLEDGMENTS

This work was financially supported by the Brain Research Center from The Featured Areas Research Center Program within the framework of the Higher Education Sprout Project by the Ministry of Education (MOE) in Taiwan and Ministry of Science and Technology (MOST) in Taiwan. S.W.C. acknowledges the generous support from MOST under grant MOST-108-2321-B-002-004 and MOST-105-2628-M-002-010-MY4, as well as from the Foundation for the Advancement of Outstanding Scholarship. K.H.L. receives funding from Academia Sinica Career Award and MOST106-2112-M-001-029. L.A.C. acknowledges the funding from MOST 106-2321-B-007-008-MY3. We thank Dr. Shung-Ming Yang and Dr. Chieh-Han Lu for the initial test of Kaede protein.

## AUTHOR CONTRIBUTIONS

H.-Y.L. and L.-A.C. developed COOL technique, including finding of blinking Kaede. H.-Y.L. and K.-H.L. helped operation of spinning disk microscope. K.-J.H. and Y.-Y.L. assisted in sample preparation and

system design. H.-Y.L. and L.-A.C. drafted the manuscript. K.-H.L., S.-W.C., and A.-S.C. designed the experiments, finalized the manuscript, and supervised the project.

## DECLARATION OF INTERESTS

The authors declare no competing interests.

Received: December 28, 2018

Revised: February 27, 2019

Accepted: March 19, 2019

Published: April 26, 2019

## REFERENCES

- Ando, R., Hama, H., Yamamoto-Hino, M., Mizuno, H., and Miyawaki, A. (2002). An optical marker based on the UV-induced green-to-red photoconversion of a fluorescent protein. *Proc. Natl. Acad. Sci. U S A* *99*, 12651–12656.
- Betzig, E., Patterson, G.H., Sougrat, R., Lindwasser, O.W., Olenych, S., Bonifacino, J.S., Davidson, M.W., Lippincott-Schwartz, J., and Hess, H.F. (2006). Imaging intracellular fluorescent proteins at nanometer resolution. *Science* *313*, 1642–1645.
- Chang, J.B., Chen, F., Yoon, Y.G., Jung, E.E., Babcock, H., Kang, J.S., Asano, S., Suk, H.J., Pak, N., Tillberg, P.W., et al. (2017). Iterative expansion microscopy. *Nat. Methods* *14*, 593–599.
- Chen, F., Tillberg, P.W., and Boyden, E.S. (2015a). Expansion microscopy. *Science* *347*, 543–548.
- Chen, X., Zong, W., Li, R., Zeng, Z., Zhao, J., Xi, P., Chen, L., and Sun, Y. (2016). Two-photon light-sheet nanoscopy by fluorescence fluctuation correlation. *Nanoscale* *8*, 9982–9987.
- Dertinger, T., Colyer, R., Iyer, G., Weiss, S., and Enderlein, J. (2009). Fast, background-free, 3D super-resolution optical fluctuation imaging (SOFI). *Proc. Natl. Acad. Sci. U S A* *106*, 22287–22292.
- Diezmann, A.V., Shechtman, Y., and Moerner, W.E. (2016). Three-dimensional localization of single molecules for super-resolution imaging and single-particle tracking. *Chem. Rev.* *117*, 7244–7275.
- Dubnau, J., Chiang, A.S., Grady, L., Barditch, J., Gossweiler, S., McNeil, J., Smith, P., Buldoc, F., Scott, R., Certa, U., et al. (2003). The *staufen/pumilio* pathway is involved in *Drosophila* long-term memory. *Curr. Biol.* *13*, 286–296.
- Fox-Roberts, P., Marsh, R., Pfisterer, K., Jayo, A., Parsons, M., and Cox, S. (2017). Local dimensionality determines imaging speed in localization microscopy. *Nat. Commun.* *8*, 13558.
- Huang, B., Babcock, H., and Zhuang, X. (2010). Breaking the diffraction barrier: super-resolution imaging of cells. *Cell* *143*, 1047–1058.
- Jones, S.A., Shim, S.H., He, J., and Zhuang, X.W. (2011). Fast, three-dimensional super-resolution imaging of live cells. *Nat. Methods* *8*, 499–505.
- Ke, M.-T., Nakai, Y., Fujimoto, S., Takayama, R., Yoshida, S., Kitajima, T.S., Sato, M., and Imai, T. (2016). Super-resolution mapping of neuronal circuitry with an index-optimized clearing agent. *Cell Rep.* *14*, 2718–2732.
- Ku, T., Swaney, J., Park, J.Y., Albanese, A., Murray, E., Cho, J.H., Park, Y.G., Mangena, V., Chen, J.P., and Chung, K.H. (2016). Multiplexed and scalable super-resolution imaging of three-dimensional protein localization in size-adjustable tissues. *Nat. Biotechnol.* *34*, 973–981.
- Lee, J., Miyayama, Y., Ueda, M., and Hohng, S. (2012). Video-rate confocal microscopy for single-molecule imaging in live cells and superresolution fluorescence imaging. *Biophys. J.* *103*, 1691–1697.
- Liu, Y.C., and Chiang, A.S. (2003). High-resolution confocal imaging and three-dimensional rendering. *Methods* *30*, 86–93.
- Pai, T.P., Chen, C.C., Lin, H.H., Chin, A.L., Lai, J.S.Y., Lee, P.T., Tully, T., and Chiang, A.S. (2013). *Drosophila* ORB protein in two mushroom body output neurons is necessary for long-term memory formation. *Proc. Natl. Acad. Sci. U S A* *110*, 7898–7903.
- Rust, M.J., Bates, M., and Zhuang, X.W. (2006). Sub-diffraction-limit imaging by stochastic optical reconstruction microscopy (STORM). *Nat. Methods* *3*, 793–795.
- Sahl, S.J., Hell, S.W., and Jakobs, S. (2017). Fluorescence nanoscopy in cell biology. *Nat. Rev. Mol. Cell Biol.* *18*, 685–701.
- Schnorrenberg, S., Grotjohann, T., Vorbruggen, G., Herzog, A., Hell, S.W., and Jakobs, S. (2016). In vivo super-resolution RESOLFT microscopy of *Drosophila melanogaster*. *Elife* *5*, e15567.
- Schropp, M., Seebacher, C., and Uhl, R. (2017). XL-SIM: extending superresolution into deeper layers. *Photonics* *4*, 33.
- Schueder, F., Lara-Gutierrez, J., Beliveau, B.J., Saka, S.K., Sasaki, H.M., Woehrstein, J.B., Strauss, M.T., Grabmayr, H., Yin, P., and Jungmann, R. (2017). Multiplexed 3D super-resolution imaging of whole cells using spinning disk confocal microscopy and DNA-PAINT. *Nat. Commun.* *8*, 2090.
- Takasaki, K.T., Ding, J.B., and Sabatini, B.L. (2013). Live-cell superresolution imaging by pulsed STED two-photon excitation microscopy. *Biophys. J.* *104*, 770–777.
- Uno, S.-n., Kamiya, M., Yoshihara, T., Sugawara, K., Okabe, K., Tarhan, M.C., Fujita, H., Funatsu, T., Okada, Y., Tobita, S., et al. (2014). A spontaneously blinking fluorophore based on intramolecular spirocyclization for live-cell super-resolution imaging. *Nat. Chem.* *6*, 681–689.
- Urban, N.T., Willig, K.I., Hell, S.W., and Nagerl, U.V. (2011). STED nanoscopy of actin dynamics in synapses deep inside living brain slices. *Biophys. J.* *101*, 1277–1284.
- Vaziri, A., Tang, J., Shroff, H., and Shank, C.V. (2008). Multilayer three-dimensional super resolution imaging of thick biological samples. *Proc. Natl. Acad. Sci. U S A* *105*, 20221–20226.
- Weisenburger, S., Boening, D., Schomburg, B., Giller, K., Becker, S., Griesinger, C., and Sandoghdar, V. (2017). Cryogenic optical localization provides 3D protein structure data with Angstrom resolution. *Nat. Methods* *14*, 141–144.
- Yamanaka, M., Yonemaru, Y., Kawano, S., Uegaki, K., Smith, N.I., Kawata, S., and Fujita, K. (2013). Saturated excitation microscopy for sub-diffraction-limited imaging of cell clusters. *J. Biomed. Opt.* *18*, 126002.
- Yu, W.T., Ji, Z.H., Dong, D.S., Yang, X.S., Xiao, Y.F., Gong, Q.H., Xi, P., and Shi, K.B. (2016). Super-resolution deep imaging with hollow Bessel beam STED microscopy. *Laser Photon Rev.* *10*, 147–152.
- Zanacchi, F.C., Lavagnino, Z., Donnorso, M.P., Del Bue, A., Furia, L., Faretta, M., and Diaspro, A. (2011). Live-cell 3D super-resolution imaging in thick biological samples. *Nat. Methods* *8*, 1047–1049.
- Zhu, D., Larin, K.V., Luo, Q.M., and Tuchin, V.V. (2013). Recent progress in tissue optical clearing. *Laser Photon Rev.* *7*, 732–757.



**ISCI, Volume 14**

**Supplemental Information**

**Imaging through the Whole Brain  
of *Drosophila* at  $\lambda/20$  Super-resolution**

**Han-Yuan Lin, Li-An Chu, Hsuan Yang, Kuo-Jen Hsu, Yen-Yin Lin, Keng-Hui Lin, Shi-Wei  
Chu, and Ann-Shyn Chiang**

## SUPPLEMENTAL INFORMATION

### Imaging through the whole brain of *Drosophila* at $\lambda/20$ super-resolution

Han-Yuan Lin<sup>a,#</sup>, Li-An Chu<sup>b,c,#</sup>, Hsuan Yang<sup>c</sup>, Kuo-Jen Hsu<sup>a,b</sup>, Yen-Yin Lin<sup>b</sup>, Keng-Hui Lin<sup>c,\*</sup>, Shi-Wei Chu<sup>a,d,\*</sup>, and Ann-Shyn Chiang<sup>b,c,e,f,g,\*</sup>

#### Supplemental Figures

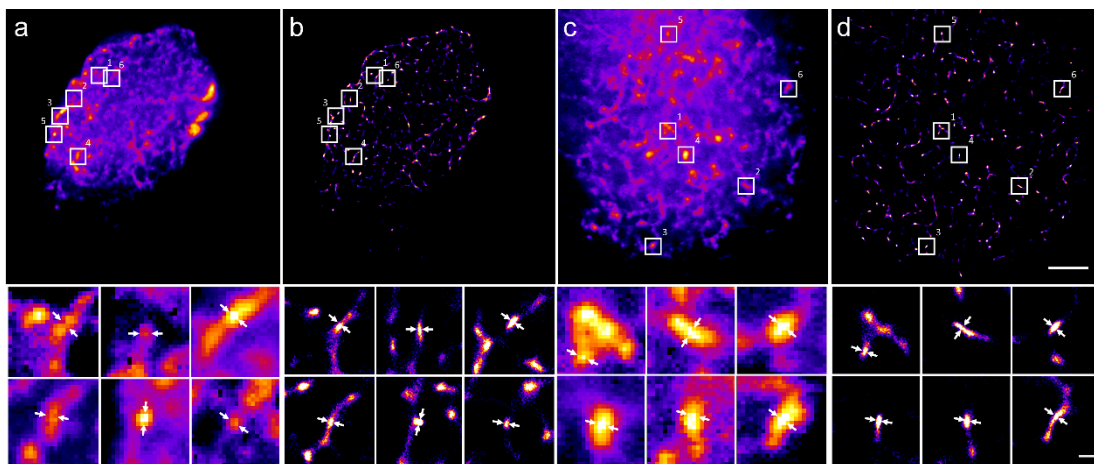


**Fig. S1 Cross-sectional resolution analysis of confocal and COOL, related to Figure 1(d-i).**

(a) confocal image at  $5\mu\text{m}$  depth (b) COOL image at  $5\mu\text{m}$  depth (c) confocal image at  $160\mu\text{m}$  depth (d) COOL image at  $160\mu\text{m}$  depth. White squares in the top row are individually magnified in the bottom row, and the arrows in the bottom lines are locations to analyze full-width-at-half-maximum (FWHM). The results are given in Table S1, showing greatly enhanced spatial resolution with COOL throughout the whole brain. Scale bar:  $5\mu\text{m}$  (top row),  $500\text{nm}$  (bottom row).

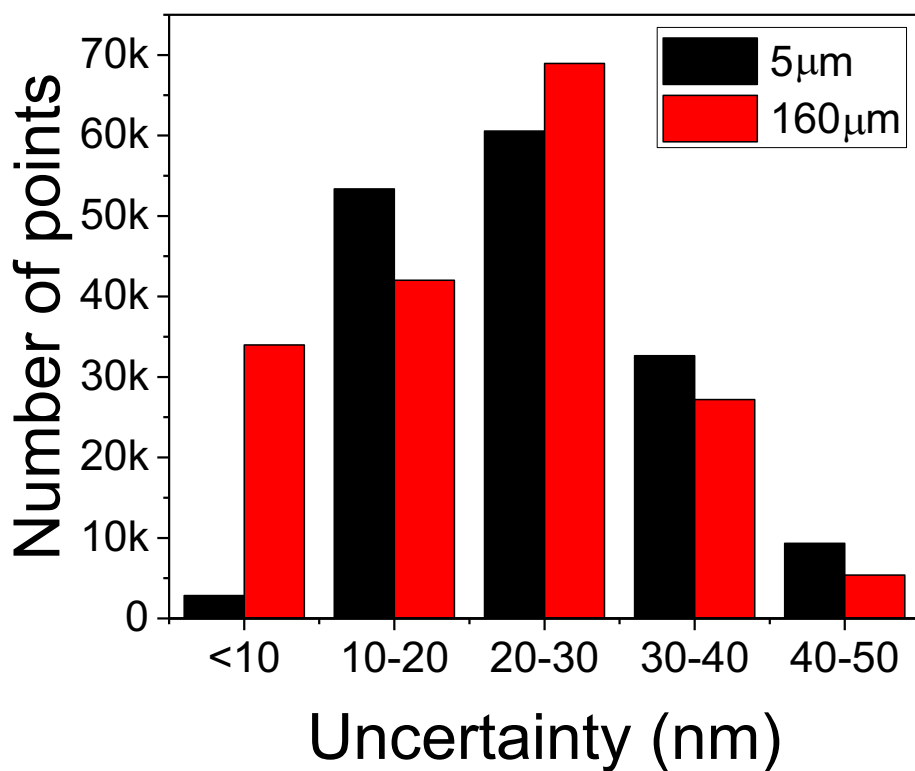


**Fig. S2 Statistics of localization uncertainty, related to Figure 1(f) and 1(i).** Histogram of the localization precisions of all recorded data at 5μm (black) and 160μm (red) depth. The corresponding average values at 5μm and 160μm are  $25.2 \pm 9.8$  nm and  $21.6 \pm 10.1$  nm, respectively.

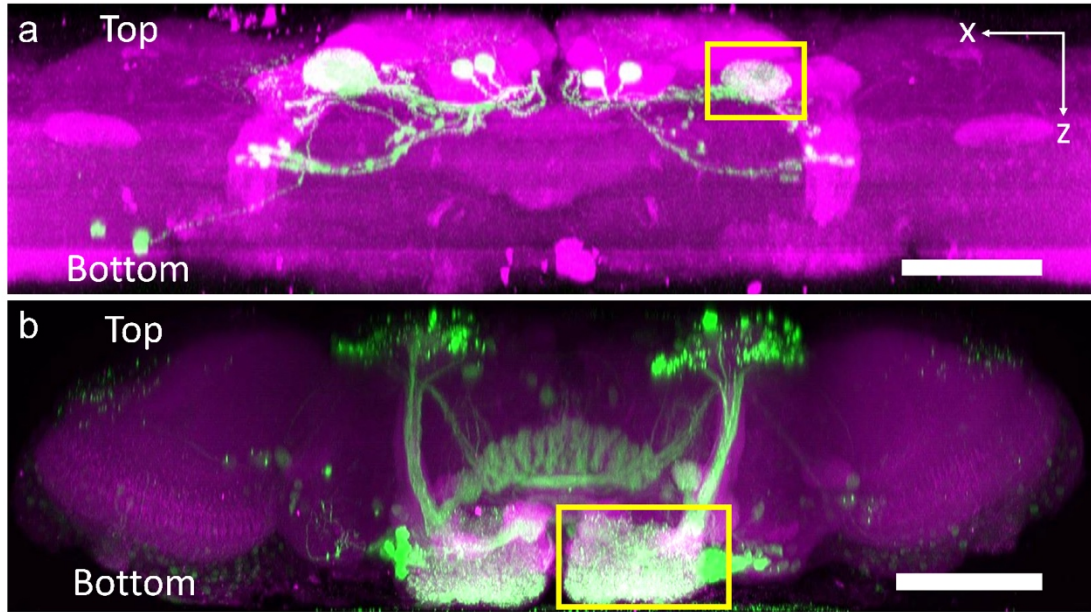


**Fig. S3 The location of *G0239-Gal4* and *krasavietz-Gal4* neurons, related to Figure 1(d-i).**

xz projection images of (a) *G0239-Gal4* neurons and (b) *krasavietz-Gal4* neurons, showing how they extend to a large volume inside a *Drosophila* brain. The yellow squares in (a) and (b) indicate the dendritic networks that correspond to Fig. 1(d,e) and Fig. 1(g,h), respectively. The former is close to brain surface, while the latter is at the bottom of brain. scale bar: 100 $\mu$ m.

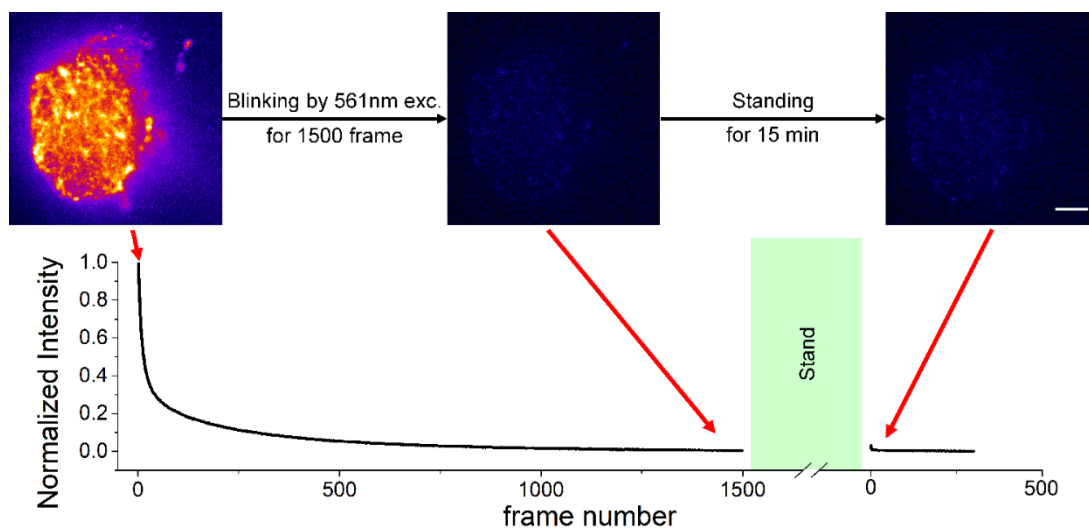


**Fig. S4.** Control experiment showing that the red-form Kaede does not increase without 405nm illumination during inter-trial standing. Scale bar: 5 $\mu$ m. This is related to Figure 1(I).

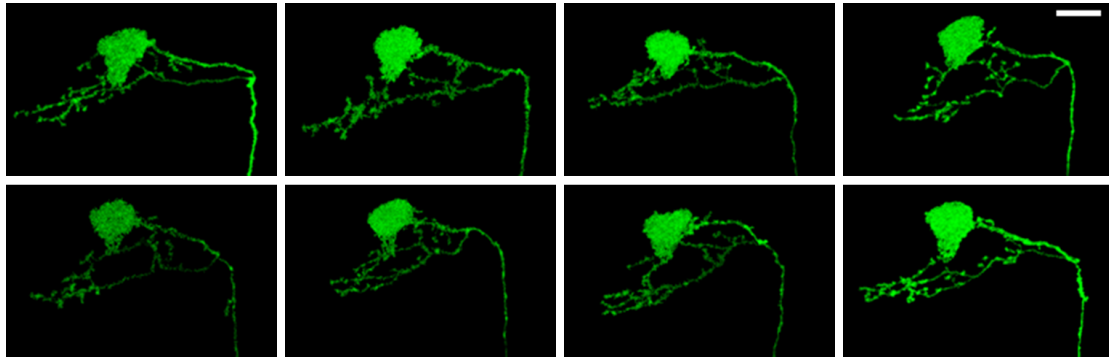


**Fig. S5 Individual variability of V3 neurons across 8 animals, related to Figure 2(c).**

When there are only 2 V3 neurons expressing in each side of brain, we showed here that 8 right brain V3 neurons from 8 different individuals exhibit different shapes of dendrite innervation areas (images from MARCM flipped single V3 neurons in Flycircuit database <http://flycircuit.tw>). These data indicate that, due to the individual variability, dendritic arbor of V3 neurons are different in each animal. Therefore, although one ideal approach to confirm the segmentation correctness in Fig. 2c is to compare with electron microscopy (EM) image of the same neuronal arbor, which can be found in (Takemura et al., 2017), due to individual variation, the side-by-side comparison is not effective.

On the other hand, the EM image does help to verify the diameter of dendritic branches measured by COOL. The EM image of the same V3 neurons was previously published in Fig. S4c of (Pai et al., 2013). It shows that the dendrite diameter is on the order of 100 nm or less, agreeing well with what we have observed in Fig. 2.

Please note that as shown by the eight confocal images of the same neuron, the dendrite network inside the neuronal arbor cannot be distinguished at all. The neural tracing capability of COOL in Fig. 2c is apparently much better than state-of-the-art confocal microscopy. Scale bar: 20 $\mu$ m.

## Supplemental Tables

	FWHM (nm) of confocal image at 5 $\mu$ m	FWHM (nm) of COOL image at 5 $\mu$ m	FWHM (nm) of confocal image at 160 $\mu$ m	FWHM (nm) of COOL image at 160 $\mu$ m
1	385	86.7	353	78.4
2	438	75.8	490	81.9
3	411	81.7	520	80.5
4	464	76.3	538	75.4
5	394	78.9	488	99.6
6	355	85.5	474	88.3
Average	408	80.8	477	84.0
Standard Deviation	35	4.2	60	8.0

**Table S1. FWHM statistics, related to Figure 1(f) and 1(i).**

The table gives the Gaussian-fitted FWHMs corresponding to different cross-sections (the bottom row) of Fig. S1. The average and standard deviation are given in the last two rows.

## Transparent Methods

### **Fly stocks**

Fly stocks were raised on cornmeal food at 25 °C and 70% relative humidity under a 12:12-h light/dark cycle. The following fly lines were used in the current study: *G0239-Gal4* (Pai et al., 2013) (16239, Bloomington Stock Center) and *krasavietz-Gal4* (Dubnau et al., 2003) were used to label *Drosophila* brain neurons; UAS-kaede (Ando et al., 2002) (26161, Bloomington Stock Center, RRID:DGGR\_109667) was used as expressing kaede protein in Gal4 labeled neurons.

### **Brain sample preparation**

Fly brains were dissected in phosphate-buffered saline (PBS, pH 7.2) and immediately transferred to a microwave-safe 24-well plate containing 4% paraformaldehyde in PBS. The plate was placed on shakers for 25 min. Fixed tissues were then permeabilized and blocked by incubating in PBS containing 2% Triton X-100 and 10% normal goat serum (NGS; Vector Laboratories, Burlingame, CA) at 4°C overnight. Fly brains then mounted in FocusClear™ (CelExplorer, FC-101) medium, with 0.7% of  $\beta$ -mercaptoethanol ( $\beta$ ME) (Sigma-Aldrich M6250) 24~48 hrs before imaging, to enhance fluorophore survival rate as well as maximal number of switching cycles. (Dempsey et al., 2011)



## **Characterizing blinking property of Kaede**

As a blinking probe, it is important to characterize the physical properties of Kaede, e.g. mean switching cycles, the on-off duty cycle, and survival fraction. Here, the analysis was based on an image sequence with 250 ms exposure time per frame and in total 2000 frames, i.e. 500 s total recording time.

To obtain switching cycles, we had to determine the total on-state time of a single fluorescent molecule, divided by how long individual blink event lasts. To identify how long individual blink event lasts, we used “Merging” function of ThunderSTORM (ImageJ plugin)(Ovesny et al., 2014). The average blinking time and the total on-state time were found to be 258 ms and 800 ms, respectively. Therefore, the average switching cycles was  $800 / 258 = 3.1$ .

For the on-off duty cycle, it was determined by dividing the total on-state time by the total recording time, i.e.  $800 \text{ ms} / 500 \text{ s} = 0.0016$ . We then calculated the survival fraction of Kaede, which was derived from the ratio of blinking event number in the 2000th frame (102) to that in the first frame (515), leading to 0.198 survival fraction after 500 s illumination.

Compared to other yellow-absorbing organic dyes (Dempsey et al., 2011), such as Cy3 and Alexa Fluor 568, their mean switching cycle are 1.6 and 52, mean duty-

cycle are 0.0003 and 0.0027, and survival fraction after 400 s are 0.55 and 0.99, respectively. Please note that these characterizations were performed with purified dyes on coverslip. In our case, genetically generated Kaede is expressed in an intact brain, and shows relatively fair performance in terms of switching cycle and duty cycle, but relatively low survival rate. The poor survival rate of Kaede might be due to high excitation intensity requirement when imaging endogenously expressed fluorescent protein.

### **Optical setup**

The images were taken with a 63x, 1.3 NA glycerol objective (PL APO HCX CS, Leica, Germany) lens mounted on a DMI6000 microscope (Leica, Germany) equipped with CSU spinning disk confocal scan head (Yokogawa, Tokyo, Japan), an objective piezo Z drive (Physik Instrumente, Karlsruhe, Germany), and an Andor 885 EMCCD (Belfast, UK) with an additional 1.2x tube lens controlled by MetaMorph (version 7.8.12.0, Molecular Devices, Sunnyvale, California, USA). With the aid of a 100 mW, 561-nm excitation source (ILE4000, Andor, UK), which fitted the excitation band of photoconverted Kaede (red form), substantial blinking was observed, allowing subsequent localization computation. Please note that no conversion of Kaede was necessary for super-resolution, so only one excitation laser was required.

For Fig. 1l, a 405-nm laser was used for converting non-blinking green-form Kaede into blinking red-form. The lasers were coupled into confocal scan head by a Borealis Perfect Illumination Delivery<sup>TM</sup> fiber, and the laser power after the objective was around 8 mW. The hardware is all commercially available, signifying a very important advantage of our technique, i.e. to advance deep-tissue super-resolution based on existing hardware.

It is interesting to note that the spinning disk system did not provide diffraction-limited resolution, probably due to the underfilled objective and intrinsic aberration in the system. Similar non-ideal resolution of spinning disk was observed recently.(Chen et al., 2015b) Since no aberration correction was included here, our result in fact reflects that localization microscopy is less sensitive to aberration, compared to wavefront engineered super-resolution techniques like SIM and STED.

The confocal images in Fig. 1 and Fig. S3 are averaged over fifty images, to improve their signal-to-noise ratio. For COOL imaging, at least 1000 images were acquired, with 3 – 4 frames/sec in speed. The localization analysis was performed via the free ImageJ plugin ThunderSTORM(Ovesny et al., 2014). OriginPro 2016 was used to illustrate Fig. 3 and curve fitting in Fig. 1(f), 1(i), 1(k).

### **Image processing with ThunderSTORM**

For proper localization results, several hardware parameters in ThunderSTORM had to be correctly set. First, the pixel size was set as 105.8 nm, which was derived from the 8  $\mu\text{m}$  CCD pixel size and the magnification ratio between the objective (63x) and the tube lens (1.2x). Second, the photoelectron per A/D count was set as 4.88, obtained from the CCD full well capacity (80,000 electrons) divided by the 14-bit digitization. Third, the base level was set as 0 since no significant background was observed during image acquisition.

There were also a number of software parameters to determine, including image filter, approximate localization methods, sub-pixel localization methods, and ways of visualization. For image filtering, “lowered Gaussian filter” was selected, with sigma set as 1.4. For approximate localization method, we chose “local maximum” method with 8-neighbourhood connectivity. The threshold of one standard deviation is used, to ensure the number of solved point is enough to show clear structure, while avoiding misinterpreted point spread functions from noise. In terms of sub-pixel localization, “integrated Gaussian” was adopted, with 3-pixel fitting radius, weighted least square, and 1.6-pixel initial sigma. The visualization condition was set as normalized Gaussian, with 10x magnification and 10-nm lateral uncertainty (Force button checked). In addition, drift correlation of ThunderSTORM was performed after visualization.

## **Manual image segmentation**

The complete 3D raw data stack of Fig. 2(c) is provided in supplementary movie S4(a). Since some structures are not continuous, similar to the situation of most super-resolution imaging, we decided to perform manual image segmentation, instead of relying on existing software. One important a priori information is that there are two G0239-Gal4 cells on each side of the brain, as shown in Fig. S3(a). The dendritic network tracking began from thick dendritic fibers (the left-hand side in the yellow rectangle of Fig. S3(a)), where we can easily identify two fibers. The branches of these two fibers are manually traced and recorded with the “Paintbrush tool” in ImageJ, to mark segments that belong to the same dendritic fiber, as shown in supplementary movie S4(b). Subsequently, the 3D marked segments were then transferred into corresponding label field in Avizo 7.1 (ThermoFisher) as a mask, and multiply with the raw confocal image to remove background while keeping the signal strength, thus generating 3D super-resolved reconstruction of the selected dendrites.

## Supplemental References

- Ando, R., Hama, H., Yamamoto-Hino, M., Mizuno, H., and Miyawaki, A. (2002). An optical marker based on the UV-induced green-to-red photoconversion of a fluorescent protein. *Proc Natl Acad Sci USA* *99*, 12651-12656.
- Chen, X., Zeng, Z., Wang, H., and Xi, P. (2015b). Three-dimensional multimodal sub-diffraction imaging with spinning-disk confocal microscopy using blinking/fluctuating probes. *Nano Res* *8*, 2251-2260.
- Dempsey, G.T., Vaughan, J.C., Chen, K.H., Bates, M., and Zhuang, X.W. (2011). Evaluation of fluorophores for optimal performance in localization-based super-resolution imaging. *Nat Methods* *8*, 1027-1036.
- Dubnau, J., Chiang, A.S., Grady, L., Barditch, J., Gossweiler, S., McNeil, J., Smith, P., Buldoc, F., Scott, R., Certa, U., *et al.* (2003). The staufen/pumilio pathway is involved in *Drosophila* long-term memory. *Curr Biol* *13*, 286-296.
- Ovesny, M., Krizek, P., Borkovec, J., Svindrych, Z.K., and Hagen, G.M. (2014). ThunderSTORM: a comprehensive ImageJ plug-in for PALM and STORM data analysis and super-resolution imaging. *Bioinformatics* *30*, 2389-2390.
- Pai, T.P., Chen, C.C., Lin, H.H., Chin, A.L., Lai, J.S.Y., Lee, P.T., Tully, T., and Chiang, A.S. (2013). *Drosophila* ORB protein in two mushroom body output neurons is necessary for long-term memory formation. *Proc Natl Acad Sci USA* *110*, 7898-7903.
- Takemura, S., Aso, Y., Hige, T., Wong, A., Lu, Z., Xu, C S., Rivlin, P. K., Hess, H., Zhao, T., Parag, T., Berg, S., Huang, G., Katz, W., Olbris, D. J., Plaza, S., Umayam, L., Aniceto, R., Chang, L.-A., Lauchie, S., Ogundeyi, O., Ordish, C., Shinomiya, A., Sigmund, C., Takemura, S., Tran, J., Turner, G. C., Rubin, G. M., Scheffer, L. K. (2017) A connectome of a learning and memory center in the adult *Drosophila* brain. *eLife* *6*, e26975.